ACS APPLIED MATERIALS & INTERFACES

www.acsami.org

Research Article

Strong Interfaces Enable Efficient Load Transfer for Strong, Tough, and Impact-Resistant Hydrogel Composites

Qiqi Xue, Yunfeng He, Xiaoyu Zhang, Xin Zhang, Minkun Cai, Chuan Fei Guo, and Canhui Yang*

Cite This: *ACS Appl. Mater. Interfaces* 2022, 14, 33797−33805

Read Online

ACCESS | Metrics & More | Article Recommendations | Supporting Information

ABSTRACT: Many biological hydrogels are mechanically robust to bear quasi-static and impact loads. In contrast, the mechanical properties of synthetic hydrogels against impact loads remain substantially unexplored, albeit their mechanical robustness under quasi-static loads has been extensively developed. Here, we report on the design and synthesis of strong, tough, and impact-resistant hydrogel composites by reinforcing Ca-alginate/polyacrylamide hydrogels with glass fabrics and conferring strong interfaces between the hydrogel matrix and the fibers. The fabric enables high elastic modulus, the hydrogel matrix enables large dissipation, and the strong interfaces enable efficient load transfer for synergistic strengthening and toughening, which is manifested by digital image correlation analyses. Under quasi-static loads, the hydrogel composite exhibits an elastic modulus of 35 MPa and a toughness of 206.7 kJ/m^2. Under impact loads, a piece of 7.7 g sample bears the impact of energy of 7.4 J and resists more than 100 cycles of consecutive impact of 600 mJ. As a proof-of-concept, a hydrogel composite as a safeguard to protect fragile glasses from impact is demonstrated. Because impact phenomena are universal, it is expected that the study on the impact of hydrogels will draw increasing attention.

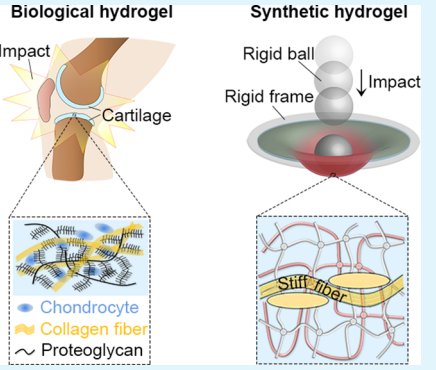

KEYWORDS: *hydrogel composite, impact resistance, tough matrix, stiff reinforcement, strong interfaces*

INTRODUCTION

Hydrogels are three-dimensional polymer networks infiltrated with a large amount of water. In this sense, many tissues of animals and plants are hydrogels. Despite the high water content, many biological hydrogels are mechanically robust and impact-resistant that they are endurant over various loads under both quasi-static and impact conditions. For instance, human cartilages possess an elastic modulus on the order of 10−100 MPa and toughness on the order of 1000 J/m^2[1−3] and cushion the human body by sustaining millions of cycles of impacts throughout the lifespan.

The exceptional mechanical performances of biological hydrogels have long been the inspiration for synthetic hydrogels.[4,5] Over the past two decades, significant progress has been made in synthesizing strong and tough hydrogels, with salient examples encompassing double-network hydrogels,[6−8] nanocomposite hydrogels,[9] topological hydrogels,[10] polyampholyte hydrogels,[11] supramolecular hydrogels,[12] and composite hydrogels.[13,14] The improvements in the mechanical properties of hydrogels have enabled numerous applications previously inaccessible such as tough tissue adhesives,[15] next-generation regenerative medicines,[16] soft machines,[17] ionotronics,[18] and bioelectronics.[19] However, existing studies mainly focus on the mechanical properties of hydrogels under quasi-static loads, and deficient attention has been paid to their impact responses.

Impact loads are pervasive in practice. For example, walking, jumping, and running repeatedly exert dynamic compressions on articular cartilages, and incidental collisions such as tumbles impose strikes on tissues. Investigating the impact responses of hydrogels promises broad applications, ranging from predicting the penetration pressure of skin by a hypodermic needle for injection administration,[20,21] to the assessment of tissue damage caused by incidents,[22,23] or chronic disease like the progression of osteoarthritis under consecutive impacts.[24] Albeit the impact responses of biological tissues have been intensively evaluated,[25−29] the examinations of the behaviors of synthetic hydrogels subjected to impact are relatively scarce.[30−33] More importantly, the synthetic hydrogels impacted so far are mostly fragile that the hydrogel may shatter into fragments after impact,[30] which is adverse for postanalysis. Because many applications of synthetic hydrogels, such as tissue-mimicking phantoms[34] and protective fabrics,[32] are readily encountered impact loads, synthesizing hydrogels that are strong and tough under not only quasi-static but also

Received: April 22, 2022
Accepted: June 29, 2022
Published: July 12, 2022

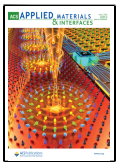

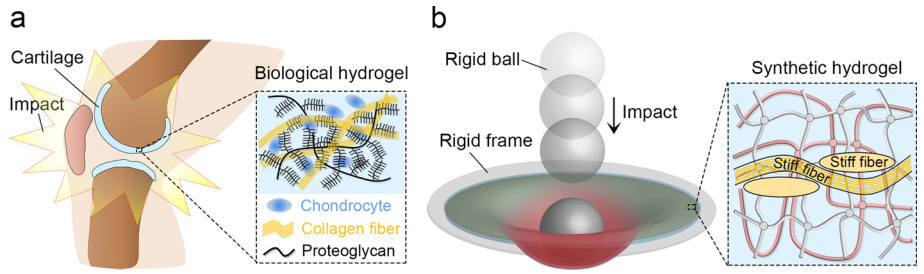

Figure 1. Bioinspired design and synthesis of a strong, tough, and impact-resistant hydrogel composite. (a) Cartilage, which consists mainly of a chondrocyte interpenetrated and collagen fiber bundles reinforced matrix of proteoglycan, is tough and impact-resistant. (b) Schematic showing a fiber-reinforced tough hydrogel composite resists impact.

impact loads and probing their impact responses are of great practical importance yet remain elusive.

In this work, we report the design and synthesis of a cartilage-inspired strong, tough, and impact-resistant hydrogel composite and assess its impact performances using low-speed impact. We reinforce the tough Ca-alginate/polyacrylamide (PAAm) hydrogel matrix with a woven fabric of glass fibers and covalently weld the interfaces between the glass fibers and the hydrogel matrix. The hydrogel composite exhibits remarkable mechanical performances under both quasi-static and impact loads, which is attributed to the efficient load transfer as manifested by digital image correlations (DICs). Moreover, the application of the hydrogel composite as a safeguard to protect fragile glasses from impact is demonstrated. Because impact phenomena are universal, it is expected that the study on the impact of hydrogels, an important but largely untilled area in the field, will draw increasing attention.

EXPERIMENTAL SECTION

Synthesis of the Ca-Alginate/PAAm Hydrogel. A two-step method is used to synthesize the Ca-alginate/PAAm hydrogels.[35] In the first step, sodium alginate (Na-alginate) polymers and acrylamide (AAm) grains (the weight ratio of alginate to acrylamide is 1:8) are dissolved in deionized water. The crosslinking agent (*N*,*N*′-methylenebisacrylamide, MBAA) and photoinitiator (α-ketoglutaric acid), of molar ratio 0.04 and 0.1 mol%, respectively, relative to acrylamide monomer, are subsequently added to obtain the Na-alginate/PAAm hydrogel precursor. Then the precursor is transferred into a mold and exposed to ultraviolet light for 2 h to generate the Na-alginate/PAAm hydrogels. In the second step, the Na-alginate/PAAm hydrogels are soaked in a 0.3 M $CaCl_2$ solution for 3 h. During the soaking, Ca^{2+} ions diffuse in and Na^+ ions diffuse out of the hydrogel network thereby ion exchange. Ca^{2+} ions interact with the carboxyl groups on different alginate chains through electrostatic interactions and crosslink the alginate network to form a double-network Ca-alginate/PAAm hydrogel. Note that both the amounts of calcium ions and MBAA have been revealed to profoundly affect the mechanical properties of the Ca-alginate/PAAm hydrogel through the crosslinking densities of the alginate network and the PAAm network, respectively,[7] and the optimized version has been utilized here without further optimizations.[35]

Synthesis of the Fiber-Reinforced Ca-Alginate/PAAm Hydrogel Composite. For the hydrogel composite with a strong interface between the glass fiber and the hydrogel matrix, the surfaces of glass fabrics are engrafted with vinyl silanes (Figure S2). Two grams of 3-(trimethoxysilyl)propyl methacrylate (TMSPMA) is dissolved in 98 g acetic acid solution (pH = 3.5) to prepare a silane solution. The glass fabric is treated with plasma for 20 min and then immediately immersed in the silane solution at room temperature for 2 h. During the submersion, the TMSPMA molecules hydrolyze and anchor onto the surfaces of glass fibers covalently through silane condensation.[36] Then the modified glass fabric is fastened in the middle of the mold followed by the infusion of the Na-alginate/PAAm hydrogel precursor. After ultraviolet illumination for 6 h, the fiber-reinforced Na-alginate/PAAm hydrogel composite is obtained. The vinyl groups of the anchored TMSPMA molecules can participate in the polymerization of the PAAm chain such that the cured Na-alginate/PAAm hydrogel is covalently adhered to the glass fabric. Thereafter, the fiber-reinforced Na-alginate/PAAm hydrogel composite is soaked in a 0.3 M $CaCl_2$ solution for 3 h to form the fiber-reinforced Ca-alginate/PAAm hydrogel composite. For comparison, the fiber-reinforced Ca-alginate/PAAm hydrogel composite without silane modification is also synthesized and characterized.

Other details regarding the synthetic process, scanning electron microscopy, tensile and tearing tests, pull-out tests of single bundle of fibers, impact tests, and cyclic loading tests are supplied in the Supporting Information.

RESULTS AND DISCUSSION

Design and Synthesis of the Hydrogel Composite. The design of the hydrogel composite is inspired by the articular cartilage, a strong, resilient, and tough tissue that provides a covering for the bones to withstand impact loads (Figure 1a). Structurally, the articular cartilage consists mainly of a polymer matrix of proteoglycan, interpenetrated with chondrocytes and collagen assemblages,[37,38] which are woven together by collagen to form a fibrous network.[39] The stiff rodlike collagen assemblages, of elastic modulus of ~1 GPa,[27] provide high tensile strength, the matrix of supermolecules provides high toughness, and the strong interfacial bonding enables efficient load transfer (collagen-proteoglycan interactions),[39] rendering marvelous impact resistance for the articular cartilage. Analogously, a strong, tough, and impact-resistant hydrogel composite contains a tough matrix, strong fibers, and robust interfaces in-between, which mimic the functions but not the anatomy of the constituents of articular cartilage. The resulting hydrogel composite is capable of resisting impact (Figure 1b).

The design principle of the hydrogel composite generally applies to material systems of various chemistries. For example, the hydrogel matrix can be a double-network hydrogel,[40,41] a polyampholyte hydrogel,[42,43] or a hydrogel/elastomer hybrid,[44] and the reinforcements can be stainless steel wires,[40] glass fabric,[13] plastic,[41] or elastomer fibers.[45,46] Here, we illustrate the principle by using the tough Ca-alginate/PAAm hydrogel as the matrix and a woven glass fabric as the reinforcement. The hydrogel matrix contains two interpenetrating networks: an alginate network ionically crosslinked by Ca^{2+} ions through electrostatic interactions and a PAAm network covalently crosslinked by MBAA.[7] Upon deformation, the PAAm network deforms and maintains the overall integrity, meanwhile transmitting high stress into the bulk, causing the alginate-calcium complex over a large volume to

https://doi.org/10.1021/acsami.2c07133
ACS Appl. Mater. Interfaces 2022, 14, 33797−33805

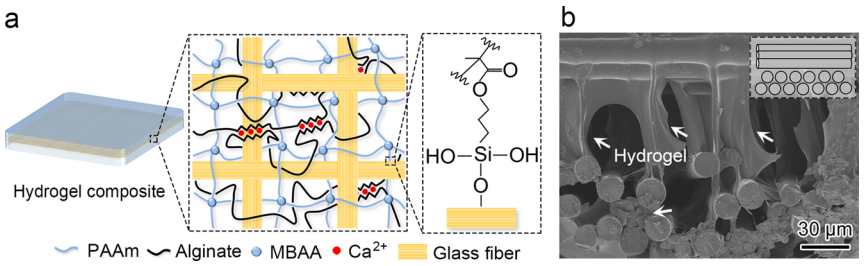

Figure 2. Hydrogel composite characterization. (a) Schematic of the hydrogel composite, consisting of a layer of glass fabric interpenetrated with the Ca-alginate/PAAm hydrogel. The PAAm chains are covalently anchored onto the surface of glass fibers via siloxane bonds. (b) Scanning electron microscopy image of the interglass fiber bundles which are filled with the polymer matrix of the hydrogel. The top-right schematic indicates the arrangement of the glass fibers.

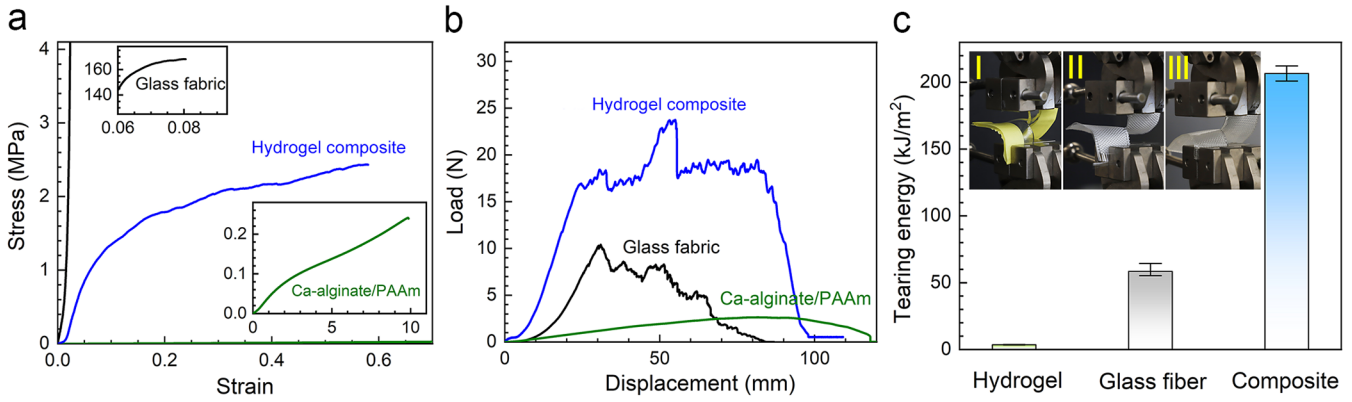

Figure 3. Quasi-static mechanical characterization. (a) Uniaxial tensile stress−strain curves at a velocity of 30 mm/min. (b) Load−displacement curves of the tearing test at 30 mm/min. (c) Tearing energy of various materials. The insets show the images of the Ca-alginate/PAAm hydrogel (I), glass fabric (II), and hydrogel composite (III) during the test.

break and dissipate enormous energy. The synergy between the two networks contributes to an extraordinarily high fracture toughness on the order of 10^4 J/m^2.[7] The glass fabric, of thickness 0.22 mm and volume fraction of ∼10%, contains orthogonally woven glass bundles, each composed of tens of 14 μm-diameter glass fibers (Figure S1a), and is topologically entangled with the Ca-alginate/PAAm hydrogel matrix (Figure 2a). In addition to the topological entanglement, we further strengthen the interfaces between the glass fibers and the hydrogel matrix by chemically anchoring the PAAm chains onto the surface of glass fibers, by engrafting vinyl silane molecules on the glass fiber through silane condensation (Figure S2). As a result, the glass fibers and the hydrogel matrix are tightly welded at the interface (Figure S1b). Hereafter, we will refer to the hydrogel composite containing strong interfaces between the matrix and the glass fibers obtained with TMSPMA treatment as the hydrogel composite with treatment, and that with weak interfaces obtained without TMSPMA treatment as the hydrogel composite without treatment. The interstitial spaces of the bundles (as indicated by the white arrows) as well as between neighboring bundles are filled by the polymers of hydrogel and the glass fabric becomes cohesive (Figure 2b).

Quasi-Static Mechanical Characterization. We first characterize the quasi-static properties of hydrogels. The Ca-alginate/PAAm hydrogel, glass fabric, and hydrogel composite possess elastic moduli of 47 kPa, 429 MPa, and 35 MPa and strengths of 240 kPa, 168 MPa, and 2.40 MPa, respectively, measured from uniaxial tension (Figure 3a). The volume fractions of the glass fabric and hydrogel matrix in the hydrogel composite are ∼10 and ∼90%, giving an elastic modulus of 43 MPa, according to the mixing rule,[47] which satisfactorily agrees with the experiment. By contrast, the elastic modulus and tensile strength of the hydrogel composite without treatment, ∼23 and ∼ 1.4 MPa (Figure S3), are much smaller, signifying the role of strong interfaces between the fibers and the matrix in the mechanical properties of the hydrogel composite.

We carry out tearing tests to measure tearing energy (Figure 3b) and obtain the values of 3.5±0.2 kJ/m^2, 58.4 ±5.2 kJ/m^2, and 206.7 ±7.6 kJ/m^2 for the Ca-alginate/PAAm hydrogel, glass fabric, and hydrogel composite (Figure 3c). Notably, the toughness of the hydrogel composite is much higher than those of the parent materials and their sum. This is because the tearing energy is predominated by two factors: the size of the energy dissipation zone and the density of energy dissipation.[48,49] For the hydrogel composite, the density of energy dissipation is related to the energy dissipation of both components, and the size of the energy dissipation zone is related to the force transfer length. On the one hand, the Ca-alginate/PAAm hydrogel provides an energy-dissipative matrix. On the other hand, given strong interfaces between components, the size of the energy dissipation zone (l_{ED}) scales with the square root of the fiber/matrix modulus ratio,[49,50] $l_{ED} \sim \sqrt{\frac{E_{fabric}}{G_{hydrogel}}}$, where E_{fabric} is the modulus of the fabric and $G_{hydrogel}$ is the shear modulus of the matrix. The fabric/matrix modulus ratio reaches ∼3 × 10^4, resulting in a large size of energy dissipation zone. Put together, the strong interface exerts a synergistic toughening mechanism to achieve high toughness.[13]

https://doi.org/10.1021/acsami.2c07133
ACS Appl. Mater. Interfaces 2022, 14, 33797−33805

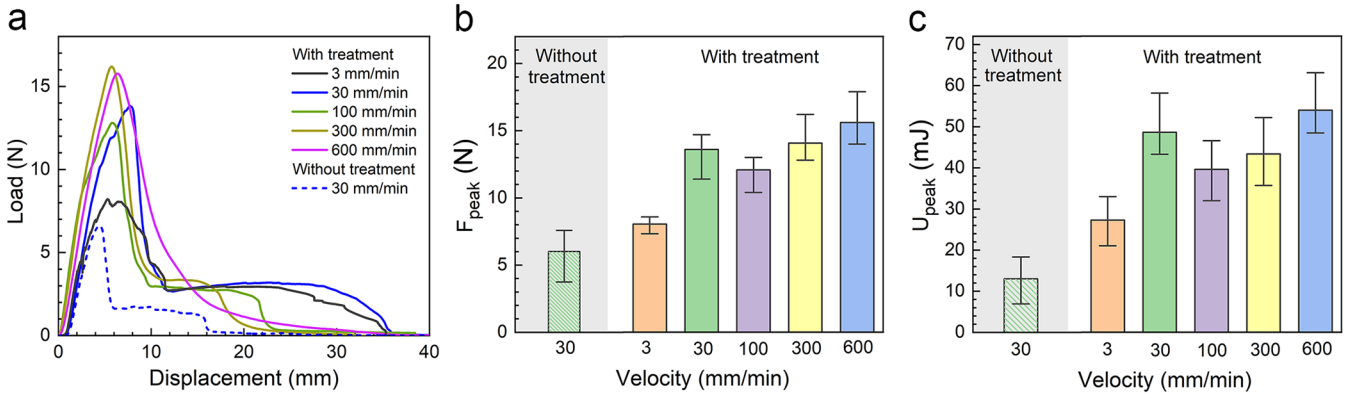

Figure 4. Pull-out tests. (a) Load−displacement curves at different loading velocities as indicated. (b) Peak pull-out force (F_{peak}) versus load velocity. (c) Peak energy absorption (U_{peak}) versus load velocity.

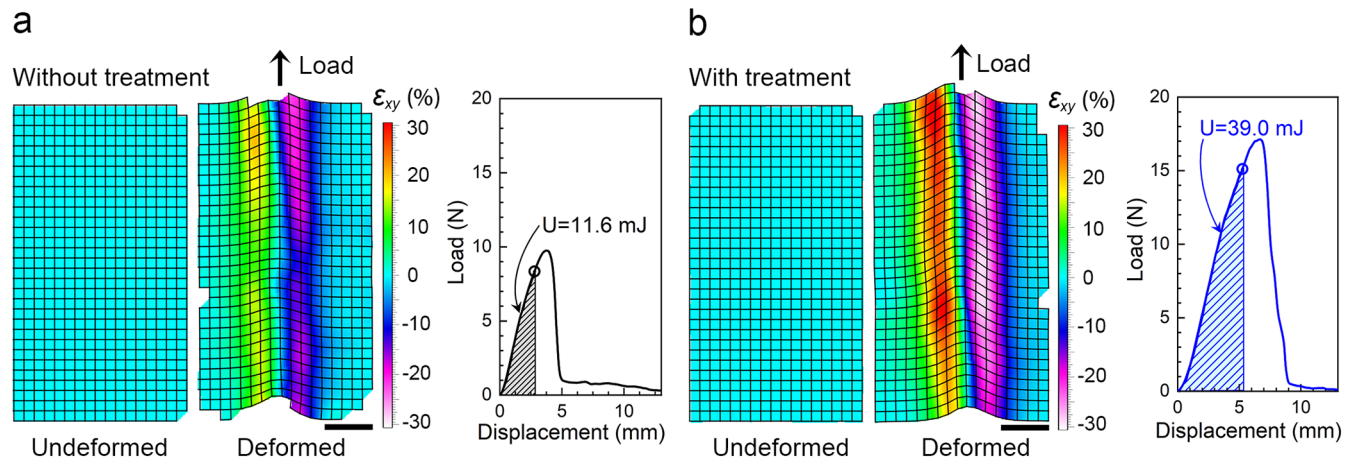

Figure 5. DIC images of pull-out tests. The samples (a) without treatment and (b) with treatment. The undeformed-state strain field corresponds to the zero-force state (A), and the deformed-state strain field corresponds to the hollow point of the load−displacement curve. ε_{xy} represents the shear strain.

To further ascertain the significance of a strong interface in the mechanical properties, we perform the fiber pull-out tests for hydrogel composites with/without treatment. As shown in Figure S4a, a single bundle of glass fibers is intercalated into the hydrogel matrix and pulled out. Five stages can be identified from the load−displacement curve: the initial state (A) where both the force and displacement are zero, the maximum force state (B) where the pull force peaks, the incipient debond state (C) where the catastrophic fracture of the hydrogel matrix surrounding the glass fiber ensues and a debond sets in, the steady debond state (D) where the debond advances under a constant force, and the complete debond state (E) where the fiber is pulled out completely. Indeed, the five stages proceed sequentially in the samples without treatment (Figure S4b) and with treatment (Figure S4c). The displacements of the samples with treatment at stages B, C, and D are much larger than those of the samples without treatment, by comparing the positions of the red, purple, and green circles in the two sets of snapshots. Worthwhile mentioning is that the occurrence of catastrophic fracture of the hydrogel matrix in the samples without treatment is earlier than that with treatment (Movie S1). Consequently, the peak force F_{peak} and the corresponding displacement D_{peak} without treatment are smaller than those with treatment. For instance, F_{peak} and D_{peak} are ∼6.8 N and ∼4 mm for the samples without treatment and are ∼14.6 N and ∼6 mm for the samples with treatment, respectively, under a loading velocity of 30 mm/min (Figure 4a). Because the Ca-alginate/PAAm hydrogel is viscoelastic, we vary loading velocity and measure the load−displacement curves (Figures 4a and S5b−S5f). Within the range of loading velocity explored, the peak force increases with loading velocity, and the peak force at 3 mm/min for the samples with treatment is still larger than the peak force at 30 mm/min for those without treatment (Figure 4b). The D_{peak} of the samples with treatment shows no dependence on loading velocity and are larger than that of the samples without treatment (Figure S5g). Considering that the hydrogel matrix is damaged after the peak force, only the performances before the peak force are concerned. We evaluate the maximum energy absorption as $U_{peak} = \int_0^{D_{peak}} F dx$. The tendency of U_{peak} is expectedly similar to that of F_{peak} (Figure 4c), with ∼14 mJ for the samples without treatment and ∼48 mJ for those with treatment. After pull-out, the trace of the samples without treatment is narrower and smoother (Figure S5h) as compared to the samples with treatment (Figure S5i). For direct visualization, we use the DIC technique to map the shear strain field during the test. The undeformed and maximum detectable deformed state of the hydrogel composites without treatment (Figure 5a) and with treatment (Figure 5b) are compared. When loaded to the maximum detectable deformed

https://doi.org/10.1021/acsami.2c07133
ACS Appl. Mater. Interfaces 2022, 14, 33797−33805

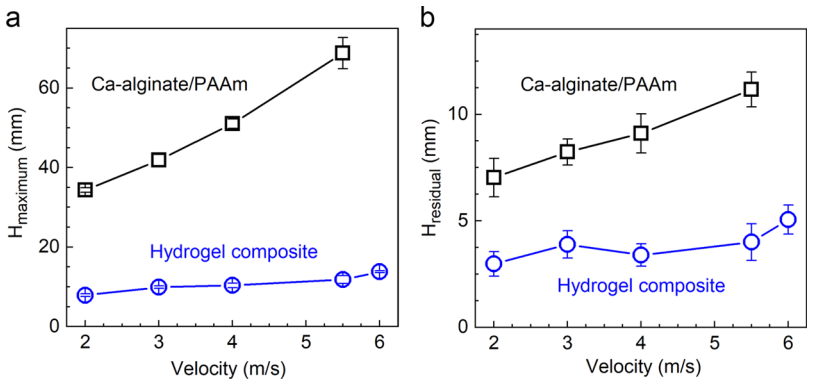

Figure 6. Monotonic impact characterization. (a) Maximum displacement ($H_{maximum}$) and (b) residual displacement ($H_{residual}$) vary with impact velocity.

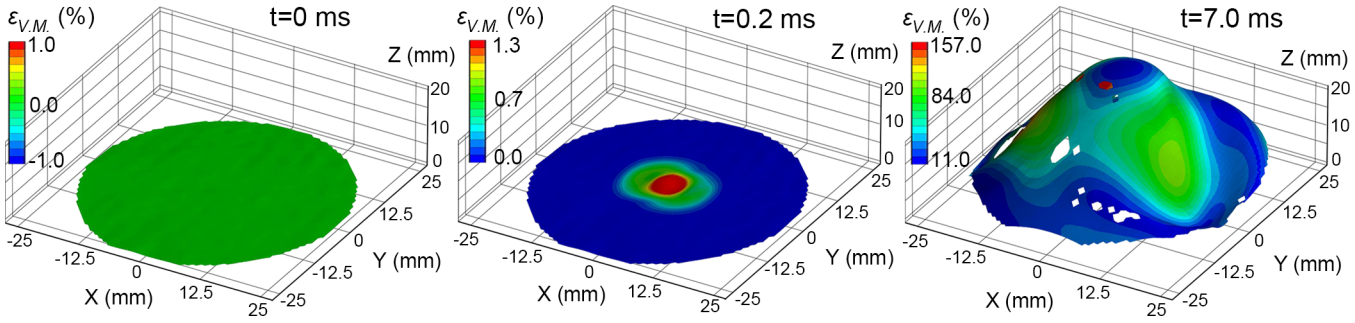

Figure 7. 3D-DIC images showing the evolution of the Von-Mises strain field under an impact velocity of 5.5 m/s for the Ca-alginate/PAAm hydrogel. The displacement along the *Z*-axis is 32 mm for the Ca-alginate/PAAm hydrogel at t = 7.0 ms.

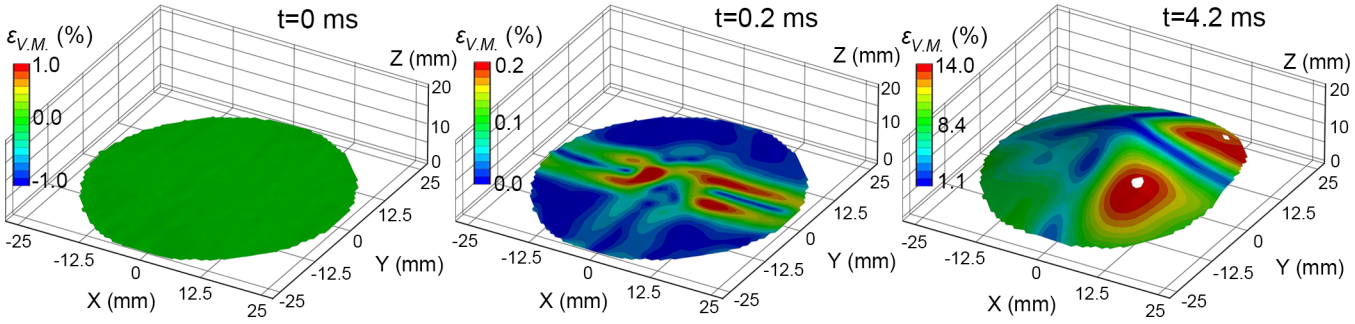

Figure 8. 3D-DIC images showing the evolution of the Von-Mises strain field under an impact velocity of 5.5 m/s for the hydrogel composite. The displacement along the *Z*-axis is 14 mm for the hydrogel composite at t = 4.2 ms.

state (the hollow point of the load−displacement curve), the size of the energy dissipation zone and the corresponding energy absorption are ∼5.5 mm and 11.6 mJ and ∼6.3 mm and 39.0 mJ for the samples without and with treatment, respectively. Although the sizes of the energy dissipation zone are similar, the corresponding energy absorption of the samples with treatment is exceedingly higher due to the efficient load transfer during deformation.

Impact Performances of Hydrogels. We then characterize the impact performances of hydrogels. We design and manufacture an apparatus for the falling ball (33.4 g steel ball) impact test (Figure S6). Subject to an impact of velocity of 2 m/s, the single-network PAAm hydrogel undergoes large deformation and fractures (Movie S2). The double-network Ca-alginate/PAAm hydrogel does not fracture, but it also undergoes large deformation with a 34 mm maximum displacement, measured as the distance from the lowest point, where the ball momentarily comes to rest, to the initial point when the ball first touches the sample. The maximum displacement increases with the impact velocity (Figure S7a) and the minimum perforation velocity for the Ca-alginate/PAAm hydrogel is about 6 m/s (Movie S3). The corresponding critical specific energy absorption is ∼177 J/kg, comparable to that of the steel plate, ∼110 J/kg,[51] but lower than that of human skin, ∼2000 J/kg,[25] by one order of magnitude. After impact, the Ca-alginate/PAAm hydrogels exhibit pronounced residual displacements, measured as the distance from the lowest point after impact to the initial point, and increases with the impact velocity as well. The large deformation of Ca-alginate/PAAm hydrogels is caused by their low elastic modulus. Under the same conditions, the hydrogel composite displays a much smaller maximum displacement (Movie S4), negligible residual displacement (Figure S7b), and imperceptible damage (Figure S8). The maximum and residual displacements against impact velocity are plotted in Figure 6a,b. At an impact velocity of 5.5 m/s, the maximum and

https://doi.org/10.1021/acsami.2c07133
ACS Appl. Mater. Interfaces 2022, 14, 33797−33805

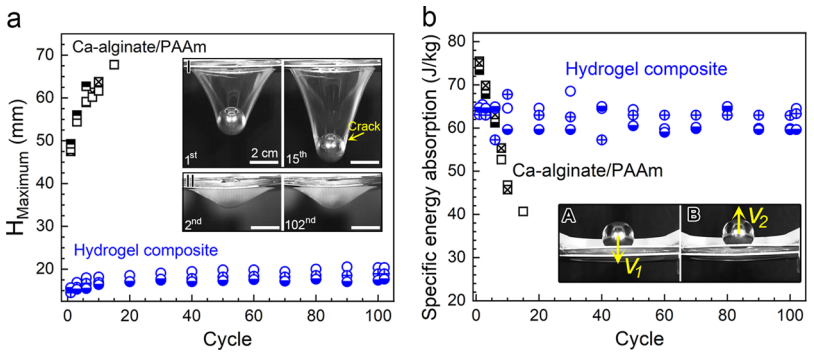

Figure 9. Cyclic impact characterization. (a) $H_{maximum}$ versus cycle of impact. At least three samples are tested. The insets show the maximum displacement for the Ca-alginate/PAAm hydrogel (I) and hydrogel composite (II) at various impact cycles as indicated. An incipient crack appears upon the 15th cycle for the Ca-alginate/PAAm hydrogel, while no observable damage is detected for the hydrogel composite upon the 102nd cycle. (b) Specific energy absorption versus the cycle of impact. Inset A: the ball hits the sample at v_1. Inset B: the ball rebounds to the same height as inset A at v_2.

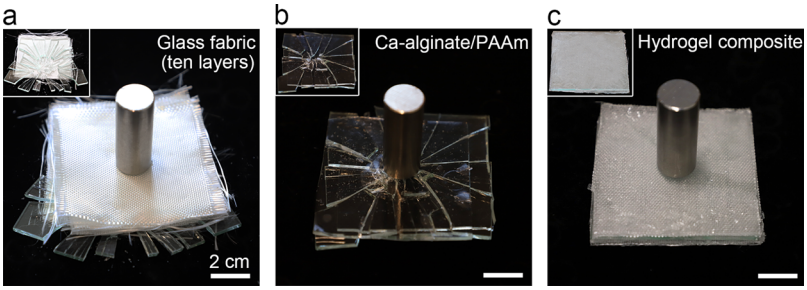

Figure 10. Applications. The photographs of (a) glass fabric, (b) Ca-alginate/PAAm hydrogel, and (c) hydrogel composite as protective materials under impact. The insets show the states of the glasses after impact.

residual displacements are 69 and 11 mm for the Ca-alginate/PAAm hydrogel and are 11 mm (a reduction of 84%) and 4 mm for the hydrogel composite. At 6 m/s, the hydrogel composite displaces by 14 mm, while the Ca-alginate/PAAm hydrogel fractures.

To scrutinize the deformation during impact, we use the 3D-DIC technique to map the full-field strain for the Ca-alginate/PAAm hydrogel (Movie S5) and hydrogel composite (Movie S6). The images showing the evolution of the Von-Mises strain field are presented in Figures 7 and 8. Before impact, the strain is zero all over the samples. Upon impact (t = 0.2 ms), the deformation of the Ca-alginate/PAAm hydrogel is exceptionally localized within a radius of ∼10 mm. At t = 7.0 ms when the Ca-alginate/PAAm hydrogel is displaced by 32 mm, which is the limit of 3D-DIC speckle recognition, the strain distribution is still nonuniform. In contrast, the deformation rapidly spreads from the impact point to the vicinity in the hydrogel composite at t = 0.2 ms and pervades the entire sample at t = 4.2 ms when the hydrogel composite is maximumly displaced, intimating that the hydrogel composite absorbs energy effectively by invoking global deformation, a merit enabled by the efficient load transfer. Because the glass fibers are pulled against the hydrogel matrix during impact, the efficient load transfer is owing to the strong interfaces between the glass fibers and the hydrogel matrix.

Many applications such as artificial cartilages require hydrogels to withstand recurring impacts. We carry out cyclic impacts with a fixed impact velocity of 6 m/s, corresponding to an impact energy of 600 mJ, for the Ca-alginate/PAAm hydrogel (Movie S7) and hydrogel composite (Movie S8). The maximum and residual displacement of the Ca-alginate/PAAm hydrogel gradually increase with the number of cycles and a crack appears upon the 15th impact (Figures S9), while the hydrogel composite remains intact after 102 cycles of impact (Figure S10) without significant changes. In particular, the Ca-alginate/PAAm hydrogel increases its maximum displacement from 48 to 65 mm before rupture, while the hydrogel composite holds a smaller maximum displacement by 70% (Figure 9a). The specific energy absorption, a pivotal factor to characterize impact resistance[52,53] and defined as the kinetic energy loss of the steel ball divided by the mass of the sample, as a function of the number of cycle is plotted in Figure 9b. Surprisingly, the hydrogel composite absorbs a comparable amount of energy with the fresh Ca-alginate/PAAm hydrogel but with much smaller deformation. As the number of cycles increases, the hydrogel composite preserves its energy absorption while the Ca-alginate/PAAm hydrogel deteriorates dramatically. To showcase the potential applications, as a proof-of-concept, we use the hydrogel composite as a safeguard to protect fragile glasses from impact. As schematized in Figure S11a, a piece of glass, 80 mm × 80 mm in area and 3 mm in thickness, is shielded between two layers of 2 mm-thick protective materials and then subjected to the impact of a 122.8-g impactor at 6 m/s. Markedly, the glass with the hydrogel composite maintains integrity while the glasses with the constituent materials as well as other common cushioning materials, such as foam and polymethyl methacrylate (PMMA) sheets, shatter into fragments after the impact (Figures 10a−c, S11b and S11c).

We note that the hydrogel composite absorbs comparable energy with the Ca-alginate/PAAm hydrogel but with much smaller deformation and further maintains stability over cyclic

https://doi.org/10.1021/acsami.2c07133
ACS Appl. Mater. Interfaces 2022, 14, 33797−33805

impact, which is abnormal because the matrix is the fatigue-prone Ca-alginate/PAAm hydrogel.[54] We interpret such a result as follows. When the samples are impacted to the maximum displacement, their momentary strains can be simplified to tensile strains (Figure S12), of ∼150 and ∼20% for the Ca-alginate/PAAm hydrogel and hydrogel composite. We conduct cyclic tensions to the corresponding strains (Figure S13) and obtain the volumetric density of energy dissipation of $\sim 2.5 \times 10^4$ J/m^3 for Ca-alginate/PAAm hydrogel and $\sim 1.6 \times 10^5$ J/m^3 for the hydrogel composite. We also measure the energy dissipation of glass fabric by loading it to the same stress of the hydrogel composite and obtain the value of $\sim 1.5 \times 10^3$ J/m^3. Resulting from the synergistic toughening,[13] the energy dissipation of the hydrogel composite is much greater than the sum of the two constituents. On the other hand, the magnitude of stress will escalate and the Ca-alginate/PAAm matrix may become more and more elastic as the strain rate increases. We implement 100 cycles of load and unload with increasing strain rate (Figure S14). Although the energy dissipation drops acutely, it plateaus after 10 cycles and the stabilized value increases with the strain rate. Linear extrapolation engenders a stabilized energy dissipation on the order of 10^5 J/m^3 at 232 s^{-1}, which is the maximum strain rate detected at an impact velocity of 5.5 m/s (Figure S15). As for the molecular scale dissipation mechanism, we charge upon the ionic crosslinks of the alginate network and the siloxane bonds between the PAAm network and glass fibers (Figure S16). The unzipping of Ca^{2+} ions from alginate chains is disastrous under large deformation, but rapid local rezipping may become possible under small deformation.[7,55] The siloxane bonds are reversible in the presence of water.[56−58] As such, it is possible that the ionic crosslinks and siloxane bonds break to dissipate energy and reform to regain the energy dissipation capability repeatedly, and a dynamic equilibrium is attained between the dynamics of bonds and the cyclic impact so that the impact performances of the hydrogel composite stabilize.

Recall that the hydrogel composite includes a tough hydrogel matrix, a stiff glass fabric, and a strong interface. First, we exclude the confounding effects of the neat fabric by impacting it at a velocity of 6 m/s. Both the maximum and residual displacement gradually increase under cyclic impact, and the braided structure is impaired after the fourth impact (Figure S17). The glass fabric by itself is not impact-resistant. Second, for a piece of fiber-reinforced PAAm hydrogel, fracture of the hydrogel matrix occurs at the first impact of 6 m/s (Movie S9), implying that a tough matrix is imperative for an impact-resistant hydrogel composite. Third, under the impact of an impactor of 412.6 g and a velocity of 6 m/s (Movie S10), the hydrogel composite without treatment exhibits larger maximum and residual displacements and fractures with the glass fibers being pulled out, while the hydrogel composite with treatment remains integral (Figure S18), implying that its critical specific energy absorption is higher than 961 J/kg. Mechanical interlocking alone is not adequate for superb impact resistance and again the role of strong interface is verified. Therefore, a strong, tough, and impact-resistant hydrogel composite dictates a tough matrix, a stiff reinforcement, and a strong interface.

CONCLUSIONS

In summary, we report a hydrogel composite that is strong and tough under both quasi-static and impact loads, by integrating the Ca-alginate/PAAm hydrogel with a glass fabric. We identify three key factors for the marvelous mechanical performances: a tough hydrogel matrix, a stiff reinforcement, and a strong interface and conduct both quasi-static and impact tests to show the marked performances of the resulting hydrogel composite. We envision that the studies of hydrogels under impact loads will gain increasing attention in light of the universality of impact loads.

ASSOCIATED CONTENT

Supporting Information

The Supporting Information is available free of charge at https://pubs.acs.org/doi/10.1021/acsami.2c07133.

Details regarding experimental section, characterization of structures and morphologies, additional results of mechanical characterization, and movies (PDF)
Fiber pull-out test (AVI)
Impact of the polyacrylamide hydrogel (AVI)
Impact of the Ca-alginate/PAAm hydrogel (AVI)
Impact of the hydrogel composite (AVI)
3D-DIC of the Ca-alginate/PAAm hydrogel under impact (AVI)
3D-DIC of the hydrogel composite under impact (AVI)
Cyclic impact of the Ca-alginate/PAAm hydrogel (AVI)
Cyclic impact of the hydrogel composite (AVI)
Impact of the fiber-reinforced PAAm hydrogel (AVI)
Impact of the hydrogel composite with/without treatment under a large mass impactor (AVI)

AUTHOR INFORMATION

Corresponding Author

Canhui Yang − *Shenzhen Key Laboratory of Soft Mechanics and Smart Manufacturing, Department of Mechanics and Aerospace Engineering, Southern University of Science and Technology, Shenzhen, Guangdong 518055, P.R. China*; orcid.org/0000-0001-5674-834X; Email: yangch@sustech.edu.cn

Authors

Qiqi Xue − *Shenzhen Key Laboratory of Soft Mechanics and Smart Manufacturing, Department of Mechanics and Aerospace Engineering, Southern University of Science and Technology, Shenzhen, Guangdong 518055, P.R. China*

Yunfeng He − *Shenzhen Key Laboratory of Soft Mechanics and Smart Manufacturing, Department of Mechanics and Aerospace Engineering, Southern University of Science and Technology, Shenzhen, Guangdong 518055, P.R. China*

Xiaoyu Zhang − *Structural Dynamic and Impact Lab, Department of Mechanics and Aerospace Engineering, Southern University of Science and Technology, Shenzhen, Guangdong 518055, P.R. China*

Xin Zhang − *Structural Dynamic and Impact Lab, Department of Mechanics and Aerospace Engineering, Southern University of Science and Technology, Shenzhen, Guangdong 518055, P.R. China*

Minkun Cai − *Department of Materials Science and Engineering, Southern University of Science and Technology, Shenzhen, Guangdong 518055, P.R. China*

Chuan Fei Guo − *Department of Materials Science and Engineering, Southern University of Science and Technology, Shenzhen, Guangdong 518055, P.R. China*

Complete contact information is available at: https://pubs.acs.org/10.1021/acsami.2c07133

https://doi.org/10.1021/acsami.2c07133
ACS Appl. Mater. Interfaces 2022, 14, 33797−33805

Author Contributions

Q.X. and C.Y. conceived the idea and designed the study. Q.X. and Y.H. prepared the sample. Q.X. and X.Z. conducted the impact tests. Q.X. and M.C. performed SEM characterization. Q.X., Y.H., X.Z., X.Z., M.C., C.G., and C.Y. analyzed and interpreted the results. Q.X. and C.Y. wrote the manuscript with the inputs from all authors. C.Y. supervised the study.

Notes

The authors declare no competing financial interest.

■ ACKNOWLEDGMENTS

The authors thank Prof. Shidi Huang from Southern University of Science and Technology for the kind assistance with a high-speed camera. This work at Southern University of Science and Technology was supported by the Natural Science Foundation of Guangdong Province (K20323004), the Stable Support Plan Program of Shenzhen Natural Science Fund Grant (K21326303), and the Science, Technology, and Innovation Commission of Shenzhen Municipality (ZDSYS20210623092005017). C.G. acknowledges the support of "Guangdong Innovative and Entrepreneurial Research Team Program" under Contract No. 2016ZT06G587 and the Shenzhen Sci-Tech Fund (No. KYTDPT20181011104007).

■ REFERENCES

(1) Simha, N. K. Evaluation of fracture toughness of cartilage by micropenetration. *J. Mater. Sci.: Mater. Med.* **2003**, *14*, 631−639.
(2) Kempson, G. E. Age-related changes in the tensile properties of human articular cartilage: a comparative study between the femoral head of the hip joint and the talus of the ankle joint. *Biochim. Biophys. Acta, Gen. Subj.* **1991**, *1075*, 223−230.
(3) Kempson, G. E. Relationship between the tensile properties of articular cartilage from the human knee and age. *Ann. Rheum. Dis.* **1982**, *41*, 508−511.
(4) Wang, W.; Zhang, Y.; Liu, W. Bioinspired fabrication of high strength hydrogels from non-covalent interactions. *Prog. Polym. Sci.* **2017**, *71*, 1−25.
(5) Fan, H.; Gong, J. P. Fabrication of bioinspired hydrogels: challenges and opportunities. *Macromolecules* **2020**, *53*, 2769−2782.
(6) Gong, J. P.; Katsuyama, Y.; Kurokawa, T.; Osada, Y. Double-network hydrogels with extremely high mechanical strength. *Adv. Mater.* **2003**, *15*, 1155−1158.
(7) Sun, J.-Y.; Zhao, X.; Illeperuma, W. R.; Chaudhuri, O.; Oh, K. H.; Mooney, D. J.; Vlassak, J. J.; Suo, Z. Highly stretchable and tough hydrogels. *Nature* **2012**, *489*, 133−136.
(8) Hua, M.; Wu, S.; Ma, Y.; Zhao, Y.; Chen, Z.; Frenkel, I.; Strzalka, J.; Zhou, H.; Zhu, X.; He, X. Strong tough hydrogels via the synergy of freeze-casting and salting out. *Nature* **2021**, *590*, 594−599.
(9) Haraguchi, K.; Takehisa, T. Nanocomposite hydrogels: A unique organic−inorganic network structure with extraordinary mechanical, optical, and swelling/de-swelling properties. *Adv. Mater.* **2002**, *14*, 1120−1124.
(10) Chang, L.; Naoya, M.; Lan, J.; Sohei, K.; Takako, N.; Hideaki, Y.; Koichi, M.; Kohzo, I. Tough hydrogels with rapid self-reinforcement. *Science* **2021**, *372*, 1078−1081.
(11) Sun, T. L.; Kurokawa, T.; Kuroda, S.; Ihsan, A. B.; Akasaki, T.; Sato, K.; Haque, M. A.; Nakajima, T.; Gong, J. P. Physical hydrogels composed of polyampholytes demonstrate high toughness and viscoelasticity. *Nat. Mater.* **2013**, *12*, 932−937.
(12) Nakahata, M.; Takashima, Y.; Yamaguchi, H.; Harada, A. Redox-responsive self-healing materials formed from host-guest polymers. *Nat. Commun.* **2011**, *2*, 1−6.
(13) Huang, Y.; King, D. R.; Sun, T. L.; Nonoyama, T.; Kurokawa, T.; Nakajima, T.; Gong, J. P. Energy-Dissipative Matrices Enable Synergistic Toughening in Fiber Reinforced Soft Composites. *Adv. Funct. Mater.* **2017**, *27*, No. 1605350.
(14) Ji, D.; Nguyen, T. L.; Kim, J. Bioinspired Structural Composite Hydrogels with a Combination of High Strength, Stiffness, and Toughness. *Adv. Funct. Mater.* **2021**, *31*, No. 2101095.
(15) Nam, S.; Mooney, D. Polymeric Tissue Adhesives. *Chem. Rev.* **2021**, *121*, 11336−11384.
(16) Slaughter, B. V.; Khurshid, S. S.; Fisher, O. Z.; Khademhosseini, A.; Peppas, N. A. Hydrogels in regenerative medicine. *Adv. Mater.* **2009**, *21*, 3307−3329.
(17) Liu, X.; Liu, J.; Lin, S.; Zhao, X. Hydrogel machines. *Mater. Today* **2020**, *36*, 102−124.
(18) Yang, C.; Suo, Z. Hydrogel ionotronics. *Nat. Rev. Mater.* **2018**, *3*, 125−142.
(19) Yuk, H.; Lu, B.; Zhao, X. Hydrogel bioelectronics. *Chem. Soc. Rev.* **2019**, *48*, 1642−1667.
(20) Shergold, O. A.; Fleck, N. A. Mechanisms of deep penetration of soft solids, with application to the injection and wounding of skin. *Proc. R. Soc. London, Ser. A* **2004**, *460*, 3037−3058.
(21) Shergold, O. A.; Fleck, N. A. Experimental investigation into the deep penetration of soft solids by sharp and blunt. *J. Biomech. Eng.* **2005**, *127*, 838−848.
(22) Ankersen, J.; Birkbeck, A. E.; Thomson, R. D.; Vanezis, P. Puncture resistance and tensile strength of skin simulants. *Proc. Inst. Mech. Eng., Part H* **1999**, *213*, 493−501.
(23) Fu, Y.; Lu, H.; Nian, G.; Wang, P.; Lin, N.; Hu, X.; Zhou, H.; Yu, H.; Qu, S.; Yang, W. Size-dependent inertial cavitation of soft materials. *J. Mech. Phys. Solids* **2020**, *137*, No. 103859.
(24) Goodwin, M.; Workman, J.; Thambyah, A.; Vanholsbeeck, F. Impact-induced cartilage damage assessed using polarisation-sensitive optical coherence tomography. *J. Mech. Behav. Biomed. Mater.* **2021**, *117*, 104326.
(25) DiMaio, V. J. Penetration and perforation of skin by bullets and missiles. *Am. J. Foren. Med. Path.* **1981**, *2*, 107−110.
(26) Lu, Y. T.; Zhu, H. X.; Richmond, S.; Middleton, J. A visco-hyperelastic model for skeletal muscle tissue under high strain rates. *J. Biomech.* **2010**, *43*, 2629−2632.
(27) Shergold, O. A.; Fleck, N. A.; Radford, D. The uniaxial stress versus strain response of pig skin and silicone rubber at low and high strain rates. *Int. J. Impact Eng.* **2006**, *32*, 1384−1402.
(28) Mijailovic, A. S.; Qing, B.; Fortunato, D.; Van Vliet, K. J. Characterizing viscoelastic mechanical properties of highly compliant polymers and biological tissues using impact indentation. *Acta Biomater.* **2018**, *71*, 388−397.
(29) McElhaney, J. H. Dynamic response of bone and muscle tissue. *J. Appl. Physiol.* **1966**, *21*, 1231−1236.
(30) Yang, J.; Li, S.; Yan, L.; Huo, D.; Wang, F. Dynamic compressive properties and failure mechanism of glass fiber reinforced silica hydrogel. *Mater. Sci. Eng., A* **2010**, *527*, 824−827.
(31) Zhang, J.; Miao, Y.; Qin, Q.; Lu, T.; Ye, Y.; He, H.; Wang, J.; Li, H. Static and dynamic experiments on hydrogels: Effects of the chemical composition of the fluid. *Mech. Mater.* **2021**, *154*, No. 103717.
(32) Ni, J.; Lin, S.; Qin, Z.; Veysset, D.; Liu, X.; Sun, Y.; Hsieh, A. J.; Radovitzky, R.; Nelson, K. A.; Zhao, X. Strong fatigue-resistant nanofibrous hydrogels inspired by lobster underbelly. *Matter* **2021**, *4*, 1755−1757.
(33) Xie, B.; Xu, P.; Tang, L.; Zhang, Y.; Xu, K.; Zhang, H.; Liu, Z.; Zhou, L.; Liu, Y.; Jiang, Z. Dynamic mechanical properties of polyvinyl alcohol hydrogels measured by double-striker electromagnetic driving SHPB system. *Int. J. Appl. Mech. Eng.* **2019**, *11*, No. 1950018.
(34) Jiang, S.; Liu, S.; Feng, W. PVA hydrogel properties for biomedical application. *J. Mech. Behav. Biomed. Mater.* **2011**, *4*, 1228−1233.
(35) Yang, C.; Wang, M.; Haider, H.; Yang, J.; Sun, J.-Y.; Chen, Y.; Zhou, J.; Suo, Z. Strengthening Alginate/Polyacrylamide Hydrogels Using Various Multivalent Cations. *ACS Appl. Mater. Interfaces* **2013**, *5*, 10418−10422.

https://doi.org/10.1021/acsami.2c07133
ACS Appl. Mater. Interfaces 2022, 14, 33797−33805

(36) Yuk, H.; Zhang, T.; Lin, S.; Parada, G. A.; Zhao, X. Tough bonding of hydrogels to diverse non-porous surfaces. *Nat. Mater.* **2016**, *15*, 190−196.
(37) Chung, C.; Burdick, J. A. Engineering cartilage tissue. *Adv. Drug Delivery Rev.* **2008**, *60*, 243−262.
(38) Fox, A. J. S.; Bedi, A.; Rodeo, S. A. The basic science of articular cartilage: structure, composition, and function. *Sports Health* **2009**, *1*, 461−468.
(39) Mow, V. C.; Holmes, M. H.; Lai, W. M. Fluid transport and mechanical properties of articular cartilage: A review. *J. Biomech.* **1984**, *17*, 337−394.
(40) Illeperuma, W. R. K.; Sun, J.-Y.; Suo, Z.; Vlassak, J. J. Fiber-reinforced tough hydrogels. *Extreme Mech. Lett.* **2014**, *1*, 90−96.
(41) Bakarich, S.; Gorkin, R.; Panhuis, M. I. H.; Spinks, G. M. Three-dimensional printing fiber reinforced hydrogel composites. *ACS Appl. Mater. Interfaces* **2014**, *6*, 15998−16006.
(42) King, D. R.; Sun, T. L.; Huang, Y.; Kurokawa, T.; Nonoyama, T.; Crosby, A. J.; Gong, J. P. Extremely tough composites from fabric reinforced polyampholyte hydrogels. *Mater. Horiz.* **2015**, *2*, 584−591.
(43) Huang, Y.; King, D. R.; Cui, W.; Sun, T. L.; Guo, H.; Kurokawa, T.; Brown, H. R.; Hui, C.-Y.; Gong, J. P. Superior fracture resistance of fiber reinforced polyampholyte hydrogels achieved by extraordinarily large energy-dissipative process zones. *J. Mater. Chem. A* **2019**, *7*, 13431−13440.
(44) Hubbard, A. M.; Cui, W.; Huang, Y.; Takahashi, R.; Dickey, M. D.; Genzer, J.; King, D. R.; Gong, J. P. Hydrogel/Elastomer Laminates Bonded via Fabric Interphases for Stimuli-Responsive Actuators. *Matter* **2019**, *1*, 674−689.
(45) Agrawal, A.; Rahbar, N.; Calvert, P. D. Strong fiber-reinforced hydrogel. *Acta Biomater.* **2013**, *9*, 5313−5318.
(46) Xiang, C.; Wang, Z.; Yang, C.; Yao, X.; Wang, Y.; Suo, Z. Stretchable and fatigue-resistant materials. *Mater. Today* **2020**, *34*, 7−16.
(47) Clyne, T. W.; Hull, D. *An introduction to composite materials*; Cambridge University Press, 2019; pp 31−32.
(48) Volokh, K.; Trapper, P. Fracture toughness from the standpoint of softening hyperelasticity. *J. Mech. Phys. Solids* **2008**, *56*, 2459−2472.
(49) Cui, W.; Daniel, R. K.; Huang, Y.; Chen, L.; Sun, T. L.; Guo, Y.; Saruwatari, Y.; Hui, C. Y.; Kurokawa, T.; Gong, J. P. Fiber-reinforced viscoelastomers show extraordinary crack resistance that exceeds metals. *Adv. Mater.* **2020**, *32*, No. 1907180.
(50) Hui, C.-Y.; Liu, Z.; Phoenix, S. L. Size effect on elastic stress concentrations in unidirectional fiber reinforced soft composites. *Extreme Mech. Lett.* **2019**, *33*, No. 100573.
(51) Jones, N.; Birch, R. Low velocity perforation of mild steel circular plates with projectiles having different shaped impact faces. *J. Pressure Vessel Technol.* **2008**, *130*, No. 031205.
(52) Sun, L.; Gibson, R. F.; Gordaninejad, F.; Suhr, J. Energy absorption capability of nanocomposites: a review. *Compos. Sci. Technol.* **2009**, *69*, 2392−2409.
(53) Beaumont, P.; Riewald, P.; Zweben, C. Methods for improving the impact resistance of composite materials. In *Foreign object impact damage to composites*; ASTM International, 1975.
(54) Bai, R.; Yang, Q.; Tang, J.; Morelle, X. P.; Vlassak, J.; Suo, Z. Fatigue fracture of tough hydrogels. *Extreme Mech. Lett.* **2017**, *15*, 91−96.
(55) Wang, J.; Mignon, A.; Snoeck, D.; Wiktor, V.; Van Vliergerghe, S.; Boon, N.; De Belie, N. Application of modified-alginate encapsulated carbonate producing bacteria in concrete: a promising strategy for crack self-healing. *Front. Microbiol.* **2015**, *6*, 1088.
(56) Plueddemann, E. P. Adhesion Through Silane Coupling Agents. *J. Adhes.* **2008**, *2*, 184−201.
(57) Taylor, D. L.; In Het Panhuis, M. Self-Healing Hydrogels. *Adv. Mater.* **2016**, *28*, 9060−9093.
(58) Xiao, Y.; Li, Q.; Yao, X.; Bai, R.; Hong, W.; Yang, C. Fatigue of amorphous hydrogels with dynamic covalent bonds. *Extreme Mech. Lett.* **2022**, *53*, No. 101679.

https://doi.org/10.1021/acsami.2c07133
ACS Appl. Mater. Interfaces 2022, 14, 33797−33805